Journal of Molecular Structure 1247 (2022) 131367

Contents lists available at ScienceDirect

Journal of Molecular Structure

journal homepage: www.elsevier.com/locate/molstr

Synthesis, crystal and molecular structure, vibrational spectroscopic, DFT and molecular docking of 4-(2-chlorobenzyl)-1-(4–hydroxy-3-((4-hydroxypiperidin-1-yl) methyl-5-methoxyphenyl)-[1,2,4] triazolo [4,3-*a*] quinazolin-5(4*H*)-one

Qingmei Wu[a,b,1], Zhaopeng Zheng[c,1], Wenjun Ye[a,b], Qian Guo[a,b], Tianhui Liao[a,b], Di Yang[a,b], Chunshen Zhao[a,b], Weike Liao[d], Huifang Chai[e], Zhixu Zhou[a,b,f,*]

[a] School of Pharmaceutical Sciences, Guizhou University, Guiyang 550025, China
[b] Guizhou Engineering Laboratory for Synthetic Drugs, Guiyang 550025, China
[c] Department of Oncology, Guizhou Provincial Peoples Hospital, Guiyang 550005, China
[d] Guizhou Provincial Engineering Technology Research Center for Chemical Drug R&D, Guizhou Medical University, Guiyang 550004, China
[e] College of Pharmacy, Guizhou University of Traditional Chinese Medicine, Guiyang, 550002, China
[f] Department of Dermatology, Affiliated Hospital of Guizhou Medical University, Guiyang 550001, China

ARTICLE INFO

Article history:
Received 17 March 2021
Revised 17 August 2021
Accepted 22 August 2021
Available online 25 August 2021

Keywords:
Triazoloquinazolinone
Crystal structure
Spectroscopy
DFT
Molecular docking

ABSTRACT

In current work, we have firstly synthesized 4-(2-chlorobenzyl)-1-(4–hydroxy-3- ((4-hydroxypiperidin-1-yl)methyl)-5-methoxyphenyl)-[1,2,4]triazolo[4,3-*a*]quinazolin-5(4*H*)-one (**1**). The structural properties of **1** were explored using spectroscopy (^{1}H NMR, ^{13}C NMR, MS and FT-IR) and X-ray crystallography method. The single-crystal structure confirmed by X-ray diffraction was consistent with the molecular structure optimized by density functional theory (DFT) calculation at B3LYP/6–311 G (2d, p) level of theory. The geometrical parameters, molecular electrostatic potential (MEP) and frontier molecular orbital (FMO) analysis were performed by DFT using the B3LYP/6–311 G (2d, p) method. Molecular docking may suggest a favorable interaction between **1** and SHP2 protein. The molecular dynamics (MD) simulation results shown that there are hydrogen bonds, electrostatic interactions and Pi interactions between compound **1** and SHP2 proteins. The inhibitory activity of **1** on SHP2 protein at 10 μM is better than the reference compound (**SHP244**).

1. Introduction

Azo heterocyclic compounds have been widely applied in pharmaceutical, textile and printing industries [1]. It's reported that the biological activities of the azo compounds including antioxidant, antibacterial, antiviral, anticancer and antitumor [2–5]. Triazoloquinazolinone as a key pharmacophore in pharmaceutical synthesis and has received considerable attention. A number of references have reported that triazoloquinazolinones have a wide range of biological activities, such as H1-antihistaminic [6–9], anticonvulsant [10], SHP2 inhibitory [11], antimicrobial [12], antitoxoplasmosis [13], anticancer and potential antivascular [14] properties.

SHP2 (encoded by PTPN11), a widely expressed non-receptor type protein tyrosine phosphatase (PTP), plays an essential role in several intracellular signal transduction processes, such as RAS-ERK, PI3K-AKT, JAK-STAT and mTOR pathways [15–17]. SHP2 is also participate in the programed cell death pathway (PD-1/PD-L1) and contribute to immune evasion [18]. SHP2 is an oncoprotein and a potential immunomodulator associated with a variety of tumor diseases, and it is also a bona fide oncogene, gain-of-function SHP2 mutations leading to increased phosphatase activity cause Noonan syndrome [19], as well as multiple forms of leukemia [20,21] and solid tumors [22,23].

In this paper, 4-(2-chlorobenzyl)−1-(4–hydroxy-3-((4-hydroxypiperidin-1-yl)methyl)−5-methoxyphenyl)-[1,2,4]triazolo [4,3-*a*]quinazolin-5(4*H*)-one (**1**) was designed based on the **SHP244** (SHP2 inhibitor) as the lead compound and synthesized for the first time. The structure of **1** was confirmed using ^{1}H NMR, ^{13}C NMR, ESI-MS and FT-IR spectra, and performed a single-crystal X-ray diffraction analysis of the crystal structure. Density functional theory (DFT) calculated optimized structure of **1** at B3LYP/6–311 G (2d, p) level of theory [24]. The geometric data,

* Corresponding author.
E-mail address: zhixuzhou@126.com (Z. Zhou).
[1] These authors contributed equally to this work.

https://doi.org/10.1016/j.molstruc.2021.131367
0022-2860/

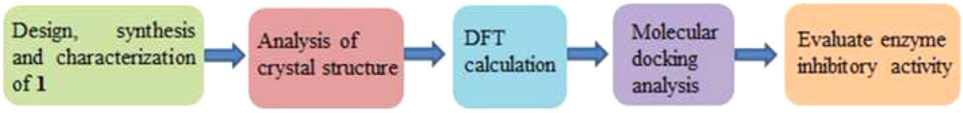

Fig. 1. Flow chart of the main points introduced in this study.

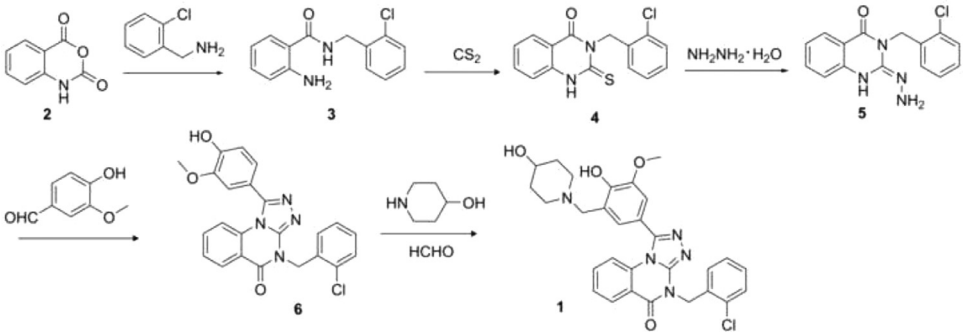

Scheme 1. Synthesis route of compound **1**.

molecular electrostatic potential (MEP), frontier molecular orbital (FMO) and vibrational property were calculated by DFT using B3LYP/6–311 G (2d, p) basis set. Analyze the ^{13}C NMR chemical shift of **1** by calculated and experimental methods. Molecular docking of molecular **1** with SHP2 protein was performed using the Surflex-Dock program in the SYBYL-X 2.0 software, and the docking study showed that molecular **1** bound to the binding site on SHP2 protein.The SHP2 enzyme inhibitory activity was evaluated at 10 μM.

2. Experimental

2.1. General remarks

All reagents and solvents for synthesis and analysis were purchased and used without further purification. ^1H NMR and ^{13}C NMR spectra were recorded by Bruker ACF-400, 400 MHz spectrometer with the tetramethylsilane (TMS) as an internal standard. Mass of **1** was taken in ESI mode on Agilent 1100 LC-MS. The FT-IR spectrum was recorded in the region of 4000 – 400 cm^{-1} with a resolution of 1.0 cm^{-1} by Bruker IFS-55 V IR spectrometer using KBr pellet technique. The melting point was determined using a digital display microscopic melting point tester. For **1**, the single-crystal X-ray diffraction data were recorded with a Bruker APEX II X-diffractometer, and collected using graphite monochromated Mo-$K\alpha$ radiation (λ = 0.71073 Å) at 100 K. The procedures used in this study are as follows: collect data: APEX2; refine cell: SAINT; solve structure: ShelXT; refine the structure and draw molecular figure: ShelXL; calculate data: DFT; calculate bond distance and bond angle: Gauss View 6.0; draw synthesis route: ChemDraw; interpret output file: Gauss View 6.0; molecular docking: SYBYL-X 2.0 software. molecular dynamics simulation: AMBERTOOL 12 software. The enzyme inhibition rate of **1** was detected with SHP2 as the target protein and **SHP244** as the positive control. Flow chart of the main points introduced in this study, as shown in Fig. 1.

2.2. Synthetic details

Compound **1** was synthesized using isatoic anhydride as a raw material by ring-opening, cyclization, substitution, aldimine condensation and Mannich reactions, as shown in Scheme 1. The molecular structure of **1** was confirmed using ^1H NMR, ^{13}C NMR, ESI-MS and FT-IR spectra, and the specific details were provided in Supplementary Materials Fig.S1-S4.

2.2.1. Synthesis of 2-amino-N-(2-chlorobenzyl)benzamide (*3*)

Isatoic anhydride (20 g, 1 eq) and ethyl acetate (200 mL) were added to a 500 mL flask, and 2-chlorobenzylamine (17.36 g, 1 eq) was added with stirring. After stirring for 2 h at 40 °C, the reaction solution was concentrated under reduced pressure, and the crude product was slurried with water, methanol and hexane to give the compound **3** (31.39 g, yield 98.2%). m.p. 108 ~ 110 °C; ^1H NMR (400 MHz, $CDCl_3$) δ: 7.47 – 7.44 (m, 1H), 7.41 – 7.37 (m, 1H), 7.34 (d, J = 7.9 Hz, 1H), 7.26 – 7.18 (m, 3H), 6.69 – 6.63 (m, 2H), 6.50 (s, 1H), 5.53 (s, 2H), 4.69 (d, J = 6.0 Hz, 2H); HRMS *m/z* Calcd for $C_{14}H_{13}ClN_2O$ $[M + H]^+$ 261.0795, found 261.0786.

2.2.2. Synthesis of 3-(2-chlorobenzyl)–2-thioxo-2,3-dihydroquinazolin-4(1H)-one (*4*)

Compound **3** (30 g, 1 eq) and ethanol (150 mL) were added to a 500 mL flask, then KOH (14.20 g, 2.2 eq) aqueous solution and CS_2 (87.61 g, 10 eq) were added with stirring. After stirring for 6 h at 55 °C, the reaction solution was cooled to room temperature. Precipitated a large amount of white solid, filtered. The filter cake was slurried with water and acetone to give the compound **4** (31.61 g, yield 90.73%). m.p. 263 ~ 265 °C; ^1H NMR (400 MHz, DMSO–d_6) δ: 13.16 (s, 1H), 7.97 (d, J = 7.5 Hz, 1H), 7.80 (t, J = 7.6 Hz, 1H), 7.48 (dd, J = 10.8, 8.5 Hz, 2H), 7.38 (t, J = 7.6 Hz, 1H), 7.28 (t, J = 7.1 Hz, 1H), 7.22 (t, J = 7.4 Hz, 1H), 6.97 (d, J = 7.4 Hz, 1H), 5.67 (s, 2H); HRMS *m/z* Calcd for $C_{15}H_{11}ClN_2OS$ $[M + H]^+$ 303.0359, found 303.0349.

2.2.3. Synthesis of (E)–3-(2-chlorobenzyl)–2-hydrazono-2,3-dihydroquinazolin-4(1H)-one (*5*)

Compound **4** (30 g, 1 eq) and isopropanol (150 mL) were added to a 500 mL flask, then 80% hydrazine hydrate (93 g, 15 eq) was added with stirring. After stirring for 16 h at 83 °C, the reaction solution was cooled to room temperature. Precipitated a large amount of white solid, filtered. The filter cake was slurried with water and *tert*–butyl methyl ether to give the compound **5** (25.62 g, yield 85.97%). m.p. 207 ~ 209 °C; ^1H NMR (400 MHz, DMSO–d_6) δ: 7.89 (d, J = 7.2 Hz, 1H), 7.62 (s, 1H), 7.49 (d, J = 7.7 Hz, 1H), 7.38 (d, J = 8.2 Hz, 1H), 7.28 (t, J = 7.2 Hz, 1H), 7.22 (t, J = 7.4 Hz, 1H), 7.10 (s, 1H), 6.79 (s, 1H), 5.22 (s, 2H), 4.43 (s, 1H); HRMS *m/z* Calcd for $C_{15}H_{13}ClN_4O$ $[M + H]^+$ 301.0856, found 301.0847.

*2.2.4. Synthesis of 4-(2-chlorobenzyl)−1-(4–hydroxy-3-methoxyphenyl)-[1,2,4]triazolo[4,3-a] quinazolin-5(4H)-one (**6**)*

Compound **5** (10 g, 1 eq) and isopropanol (200 mL) were added to a 500 mL flask, then acetic acid (0.5 mL) and 4–hydroxy-3-methoxybenzaldehyde (5.06 g, 1 eq) were added with stirring. After stirring for 0.5 h at 83 °C, the reaction solution was cooled to room temperature, and followed by $FeCl_3{\cdot\cdot}6H_2O$ (44.94 g, 5.5 eq) was added with stirring. After stirring for 1 h at 83 °C, the reaction solution was cooled to room temperature. Precipitated a small amount of brown-green solid, filtered. The filtrate was poured into water (800 mL) and after stirring for 0.5 h at room temperature, and precipitated a large amount of brown-gray solid, filtered, and the filter cake was slurried with water, acetone and *tert*–butyl methyl ether to give the compound **6** (14.20 g, yield 98.68%). m.p. 245 ∼ 247 °C; ^{1}H NMR (400 MHz, DMSO–d_6) δ: 9.76 (s, 1H), 8.26 (d, J = 7.1 Hz, 1H), 7.74 (t, J = 7.9 Hz, 1H), 7.58 – 7.53 (m, 2H), 7.34 (t, J = 6.0 Hz, 1H), 7.28 – 7.21 (m, 4H), 7.11 (d, J = 8.0 Hz, 1H), 7.02 (d, J = 8.1 Hz, 1H), 5.47 (s, 2H), 3.77 (s, 3H); HRMS *m/z* Calcd for $C_{23}H_{17}ClN_4O_3$ $[M + H]^+$ 433.1067, found 433.1056.

*2.2.5. Synthesis of 4-(2-chlorobenzyl)−1-(4–hydroxy-3-((4-hydroxypiperidin-1-yl)methyl)−5- methoxyphenyl)-[1,2,4]triazolo[4,3-a]quinazolin-5(4H)-one (**1**)*

Compound **6** (1 g, 1 eq) and acetic acid (20 mL) were added to a 500 mL flask, then 4-hydroxypiperidine (0.93 g, 4 eq) and 37% formaldehyde (0.75 g, 4 eq) were added with stirring. After stirring for 6 h at 80 °C, the reaction solution was concentrated under reduced pressure. The concentrate was poured into water and the pH was adjusted to 8 - 9 with NaOH saturated solution, and the mixed solution was extracted with dichloromethane. The combined organic layer was dried over anhydrous Na_2SO_4 and concentrated under reduced pressure. The crude product was slurried with *tert*–butyl methyl ether to give the compound **1** (0.88 g, yield 69.84%). m.p. 134 ∼ 139 °C; ^{1}H NMR (400 MHz, DMSO–d_6) δ: 8.27 (d, J = 9.3 Hz, 1H), 7.72 (t, J = 7.9 Hz, 1H), 7.59–7.53 (m, 2H), 7.37 – 7.32 (m, 1H), 7.25 (q, J = 7.9 Hz, 3H), 7.17 (s, 1H), 7.04 (s, 1H), 5.48 (s, 2H), 3.78 (s, 3H), 3.72 (s, 2H), 3.58 – 3.51 (m, 1H), 2.85–2.74 (m, 2H), 2.25 (t, J = 9.6 Hz, 2H), 1.81 – 1.72 (m, 2H), 1.43 (q, J = 10.5, 8.9 Hz, 2H); ^{13}C NMR (100 MHz, DMSO–d_6) δ:158.88, 149.17, 148.89, 148.69, 148.20, 135.04, 134.65, 133.43, 132.20, 129.80, 129.73, 129.39, 127.86, 127.79, 127.10, 123.98, 123.13, 118.40, 117.69, 116.29, 112.86, 65.91, 59.03, 56.41, 50.68, 44.25, 34.64; HRMS *m/z* Calcd for $C_{29}H_{28}ClN_5O_4$ $[M + H]^+$ 546.1908, found 546.1896.

2.3. Crystal structure determination

Compound **1** was dissolved and grown in acetonitrile at room temperature to obtain a single crystal. A colorless transparent crystal of **1** with a size of 0.15 mm × 0.08 mm × 0.05 mm was mounted on X-ray diffractometer. The single-crystal X-ray diffraction data were recorded using Bruker APEX II diffractometer, and collected the data using graphite monochromated Mo-$K\alpha$ radiation (λ = 0.71073 Å) at 170 K. A total of 15,637 reflections were collected in the range of 2.003 – 26.066° (index ranges: $-11 \le h \le 12$, $-13 \le k \le 13$, $-18 \le l \le 17$) using an φ-ω scan mode, and 5486 reflections were independent with R_{int} = 0.0826, of which 3113 observed reflections with $I > 2\sigma$ (I) were used to determinate and refine the structure [25]. The structure was solved using SHELXT-2018/3 [26], and refined using SHELXL-2018/3 [27]. The title compound **1** of the final R = 0.0754 and wR = 0.2310 ($w = 1/[\sigma^2 (F_o^2) + (0.1145P)^2 + 0.1650\ P]$, where $P = (F_o^2 + 2F_c^2)/3$), $(\Delta\rho)_{max}$ = 0.631, $(\Delta\rho)_{min}$ = −0.495 e/Å^3, $(\Delta/\sigma)_{max}$ = 0.000 and S = 1.054.

The single crystal X-ray diffraction data of **1** can be obtained free of charge via http://www.ccdc.cam.ac.uk/conts/retrieving.html (or from the Cambridge Crystallographic Data Centre, CCDC 2,050,842).

2.4. SHP2 kinase assay

The SHP2 kinase activities were evaluated using previously reported protocol [28]. Briefly, the phosphatase reactions were performed at room temperature in 384-well plate (Corning) and a final reaction volume of 25 μL, the following assay buffer conditions: 60 mM HEPES, pH 7.2, 75 mM NaCl, 75 mM KCl, 1 mM EDTA, 0.05% P-20, 5 mM DTT. 0.5 nM of SHP2 was co-incubated with of 0.5 μM of bisphosphorylated IRS1 peptide and 10 μM of **SHP244** or **1**. After 30 min incubation at 25 °C, the surrogate substrate DiFMUP (Invitrogen) was added to the reaction and incubated at 25 °C for 30 min. The reaction was then quenched by the addition of 5μL of a 160 μM solution of bpV. The plate was read using Envision (Perkin Elmer) at 340 nm and 450 nm, respectively.

3. Computational methods

3.1. DFT calculations

The DFT calculations were performed by the Gaussian 09 software package using B3LYP/6–311 G (2d, p) method, and the theoretical errors were corrected using a scaling factor of 0.961 [29]. Gauss View 6.0 program was used to calculate bond distance and bond angle. The output file was interpretated using Gauss View 6.0 program. The geometrical parameters, MEP and FMO analysis were conducted by DFT using the B3LYP/6–311 G (2d, p) method. The ^{13}C chemical shift was calculated by Gauge-Independent Atomic Orbital (GIAO) method [30].

3.2. Molecular docking

Download the SHP2 protein crystal structure (PDB: 6BMR) in the PDB protein database (https://www.rcsb.org/), then extract the required ligands use the SYBYL-X 2.0 software [31] and generate docking bag use the Surflex-Dock (SFXC) Docking mode. The structures of the compounds were created by the structure tool in SYBYL-X 2.0 software, and a conformation library was generated through force field optimization. Molecular docking of ligand molecules with SHP2 protein were performed using the Surflex-Dock suite in the SYBYL-X 2.0 software. Finally, with the help of the docking total score, the interaction between the protein and compounds was studied.

3.3. Molecular dynamics

The molecular dynamics simulation could be used to predict the drug-receptor interactions during the design phase of novel compounds development. Herein, the interaction between compound **1** and **SHP2** protein was further studied by MD simulation using AMBERTOOL 12 software [32]. Topology and parameter files were generated with the LEaP program on structure of the complexes obtained by the afore mentioned docking procedures. Analysis of MD trajectories generated was performed by Ptraj module in AMBERTOOL 12.

4. Results and discussion

4.1. Synthesis and characterization

The target compound was synthesized using five steps: ring-opening, cyclization, substitution, aldimine condensation and Mannich reactions. The structural properties of the title compound **1**

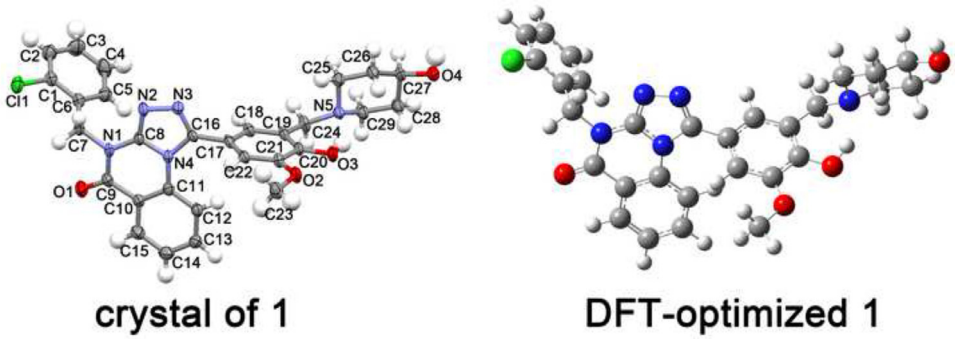

Fig. 2. The crystal and DFT-optimized structure of **1**.

Table 1
The crystal data and parameters for the structure refinement of **1**.

Compound	**1**
CCDC	2,050,842
Molecular formula	$C_{29}H_{28}ClN_5O_4$
Molecular weight	546.01
Crystal system	Triclinic
Space group	P-1
a(Å)	9.7787(12)
b(Å)	10.7815(16)
c(Å)	14.6154(16)
α (°)	88.407(4)
β (°)	74.813(4)
γ (°)	70.873(4)
V (Å^3)	1402.1(3)
Z	2
N(param)refined	355
μ (mm^{-1})	0.179
Radiation λ (Å)	0.71073
Ranges/indices (h, k, l)	$-11 \le h \le 12$, $-13 \le k \le 13$, $-18 \le l \le 17$
θ limit (°)	2.003 - 26.066
T, K	170
$N(hkl)_{measured}$, $N(hkl)_{unique}$	15,637 / 5486 [R(int) = 0.0826]
$N(hkl)_{gt}$	3113
Diffractometer	Bruker APEX II CCD'
Scan mode	φ - ω
Programs	SHELXL-2018/3

were studied using spectroscopy (^{1}H NMR, ^{13}C NMR, MS and FT-IR) and X-ray crystallography method. As shown in Supplementary Materials Fig. S1-S4.

4.2. X-ray crystallography

Crystal **1** is of triclinic system, space group P-1, with a = 9.7787(12), b = 10.7815(16), c = 14.6154(16) Å, V = 1402.1(3) Å^3, Z = 2, calculated density ρ_{calc} = 1.293 g/cm^3, and linear absorption coefficient μ = 0.179 mm^{-1}. For the target compound **1**, ORTEP diagram of the crystal and DFT-optimized structures are shown in Fig. 2.

The crystallographic and refinement data are shown in Table 1.

Analyze hydrogen bonds to further study the stability of the crystal structure [33]. For **1**, the intramolecular O(3)—H(3)···N(5) (1.866 Å), C(5)—H(5)···N(1) (2.478 Å) and C(7)—H(7B)···O(1) (2.408 Å), and the intermolecular O(4)—H(4)···N(3) (2.012 Å), C(13)—H(13)···O(4) (2.447 Å), C(23)—H(23B)···O(1) (2.595 Å) and C(27)—H(27)···Cl(1) (2.826 Å) hydrogen bonds play a major role in stabilizing the crystal structure. As shown in Table 2. Furthermore, the crystal structure is further stabilized by the van der Waals forces and π-π interactions. As shown in Fig. 3.

4.3. Conformational stability

The Spartan 08 program [34] was used to search for the initial conformation of **1**. The frequency calculations and geometry optimizations of all conformers of **1** were carried out using DFT/B3LYP/6-311 G (2d, p) in Gauss View 6.0 package. The relative Gibbs free energies $\Delta G = exp(-Gi/RT)$ (R = 8.314 J·(mol·K)$^{-1}$, T = 295.15 K) and Boltzmann distribution (Boltzmann weighting factor $Pi = \frac{exp(-Gi/RT)}{\sum_j \exp(-Gj/RT)} \times 100\,\%$) [21] of **1** are shown in Table 3.

The rotation of the C(6)-C(7) bond or the C(16)-C(17) bond causes eight conformations of **1**. The eight relatively stable conformers are **1–1** (69.10%), **1–2** (6.28%), **1–3** (5.76%), **1–4** (4.46%), **1–5** (4.32%), **1–6** (4.00%), **1–7** (3.48%), **1–8** (2.60%). As shown in Fig. 4.

The DFT-optimized structures of **1** were compared with the crystal structure obtained using X-ray diffraction. Conformer **1–1** calculated by DFT is most similar to the crystal structure, as shown in Fig. 1. Selected experimental parameters of crystal **1** were compared with the calculated parameters of conformer **1–1**. As shown in Table 4. As expected, most of the X-ray data of title compound **1** is close to the calculated geometry parameters.

4.4. Molecular electrostatic potential

Molecular electrostatic potential (MEP) is important for predicting intermolecular interactions, electrophilic attack and nucleophilic reactions [35,36]. The MEP of **1** was calculated by DFT using the B3LYP/6–311 G (2d, p) method, and the MEP diagram is shown in Fig. 5. The MEP diagram gives information on molecular shape, size, electrostatic potential value and charge distribution [37]. The MEP was recorded in the region −6.0 e^{-2} – 6.0 e^{-2}. The MEP diagram's different colors indicate different electrostatic potential values, electrostatic potential increases in the order of red < orange < yellow < green < blue. Blue represents the strongest positive potential, and red represents the strongest negative potential. The positive regions are mainly distributed around the H atoms of the phenyl, benzyl, piperidinyl and –CH_3, and these regions have a positive potential. The negative potential regions are mainly related to the N atoms of the triazole ring, the O atoms of –C = O, –OH and –OCH_3, and the Cl atom.

4.5. Frontier molecular orbital

Frontier molecular orbital (FMO) investigation is important for predicting the reactivity, site selectivity and molecular electronic transitions [38-40]. The highest occupied molecular orbital (HOMO) and lowest unoccupied molecular orbital (LUMO) energy of conformer **1–1** is calculated by DFT using B3LYP/6–311 G (2d, p). The calculated values described the catalytically and biological activity of conformer **1–1**. The frontier molecular orbital diagram is shown in Fig. 6. In LUMO, the electron cloud occupies al-

Table 2
The hydrogen-bond geometry parameters of 1.

D—H···A	*d*(D—H) /Å	*d*(H···A) /Å	*d*(D···A) /Å	∠(D—H···A) /°
O(3)—H(3)···N(5)	0.84	1.866	2.614(4)	148
O(4)—H(4)···N(3) [i]	0.84	2.012	2.820(4)	161
C(5)—H(5)···N(1)	0.95	2.478	2.840(5)	103
C(7)—H(7B)···O(1)	0.99	2.408	2.760(5)	100
C(13)—H(13)···O(4) [ii]	0.95	2.447	3.348(5)	158
C(23)—H(23B)···O(1) [iii]	0.98	2.595	3.534(5)	160
C(27)—H(27)···Cl(1) [iv]	1.00	2.826	3.675(4)	143

Symmetry code: (i) 1-x,1-y,-z; (ii) 2-x,−1-y,-z; (iii) 1-x,2-y, ι-z; (iv) $1 + x$,- $l + y$, - $l + z$.

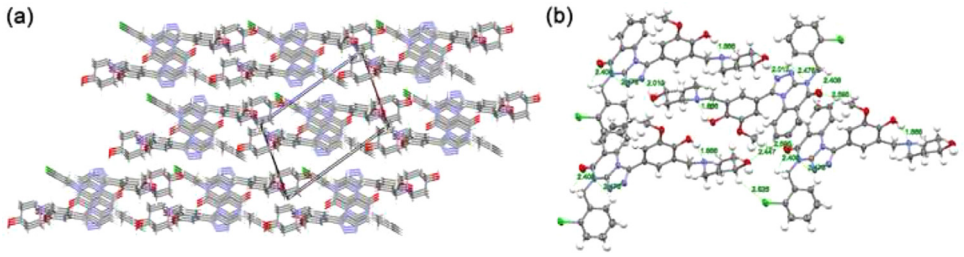

Fig. 3. The Crystal structure stacking (a) and hydrogen bond distance (b) diagram of **1**.

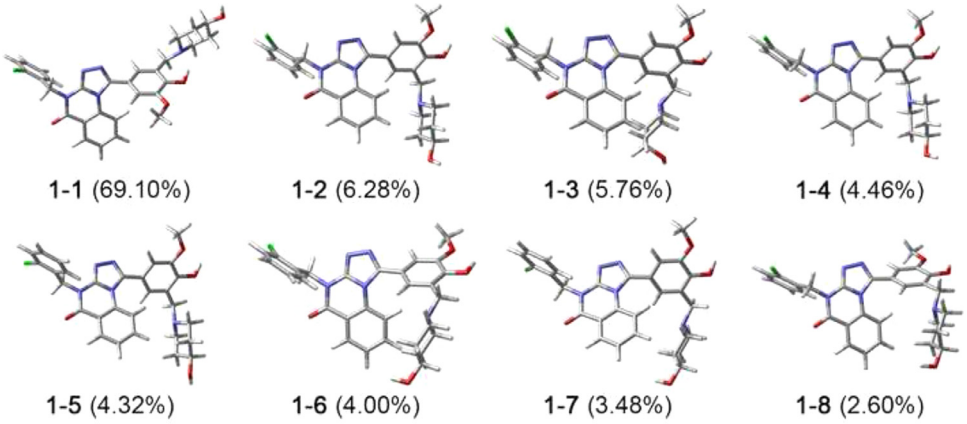

Fig. 4.. Relatively stable conformers of **1**.

Table 3
Gibbs free energy (*G*), relative Gibbs free energy (△*G*) [a] and Boltzmann weighting factor (*Pi*%) [b] of the conformers of **1**.

Conformer	*G* (kcal mol^{-1})	△*G* (kcal mol^{-1})	*Pi*%
1–1	1,353,439.156	0	69.10
1–2	1,353,437.751	1.406	6.28
1–3	1,353,437.701	1.456	5.76
1–4	1,353,437.550	1.606	4.46
1–5	1,353,437.531	1.625	4.32
1–6	1,353,437.486	1.670	4.00
1–7	1,353,437.404	1.752	3.48
1–8	1,353,437.234	1.922	2.60

[a] Related to the most stable conformer.
[b] Boltzmann weighting factor (*Pi*%) based on △*G*.

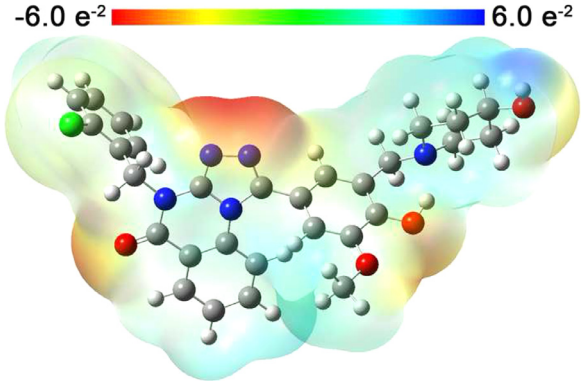

Fig. 5. Molecular electrostatic potential diagram of conformer **1–1**.

most the entire title molecule, and in HOMO, the electron cloud is mainly distributed on the triazole ring and the 1-substituted benzene ring. For conformer **1–1**, the energy values of E_{HOMO} and E_{LUMO} are −5.9699 and −1.9410 eV, respectively. The HOMO-LUMO orbital energy gap ($\triangle E = E_{HOMO} - E_{LUMO}$) is an important parameter for quantum chemistry [41]. The larger △E indicates higher chemical stability, and the smaller indicates higher reactivity [40]. For conformer **1–1**, The orbital energy gap $\triangle E = E_{HOMO} - E_{LUMO} = -4.0289$ eV. Furthermore, the electron affinity and ionization energy of conformer **1–1** can be calculated as: A = -

Table 4
Selected experimental and calculated geometry parameters for **1** and conformer **1–1**.

Bond Distances (Å)	Exp.[a]	Calcd.[b]	Difference	Bond Distances (Å)	Exp. [a]	Calcd. [b]	Difference
Cl(1)-C(1)	1.741(4)	1.763	0.022	C(12)-H(12)	0.950	1.078	0.128
O(2)-C(21)	1.370(4)	1.359	−0.011	C(12)-C(13)	1.378(5)	1.387	0.009
O(2)-C(23)	1.429(5)	1.420	−0.009	C(10)-C(15)	1.385(5)	1.397	0.012
O(3)-H(3)	0.840	0.992	0.152	C(7)-H(7A)	0.990	1.090	0.100
O(3)-C(20)	1.355(4)	1.351	−0.004	C(7)-H(7B)	0.990	1.089	0.099
O(4)-H(4)	0.840	0.964	−0.124	C(25)-H(25A)	0.990	1.091	0.101
O(4)-C(27)	1.427(4)	1.427	0.000	C(25)-H(25B)	0.990	1.104	0.114
O(1)-C(9)	1.219(4)	1.218	−0.001	C(25)-C(26)	1.518(5)	1.527	0.009
N(4)-C(8)	1.364(4)	1.376	0.012	C(1)-C(2)	1.381(6)	1.387	0.006
N(4)-C(11)	1.403(5)	1.408	0.005	C(24)-H(24A)	0.990	1.096	0.106
N(4)-C(16)	1.393(4)	1.404	0.011	C(24)-H(24B)	0.990	1.100	0.110
N(1)-C(8)	1.380(4)	1.379	−0.001	C(26)-H(26A)	0.990	1.094	0.104
N(1)-C(9)	1.386(5)	1.391	0.005	C(26)-H(26B)	0.990	1.095	0.105
N(1)-C(7)	1.465(4)	1.465	0.000	C(26)-C(27)	1.513(5)	1.528	0.015
N(5)-C(25)	1.464(5)	1.472	0.008	C(15)-H(15)	0.950	1.082	0.132
N(5)-C(24)	1.473(4)	1.474	0.001	C(15)-C(14)	1.395(6)	1.383	−0.012
N(5)-C(29)	1.472(5)	1.470	−0.002	C(27)-H(27)	1.000	1.100	0.100
N(2)-N(3)	1.400(4)	1.384	−0.016	C(27)-C(28)	1.511(5)	1.522	0.011
N(2)-C(8)	1.313(5)	1.302	−0.011	C(13)-H(13)	0.950	1.083	0.133
N(3)-C(16)	1.305(5)	1.304	−0.001	C(13)-C(14)	1.382(5)	1.395	0.013
C(21)-C(20)	1.407(5)	1.413	0.006	C(29)-H(29A)	0.990	1.092	0.102
C(21)-C(22)	1.382(5)	1.388	0.006	C(29)-H(29B)	0.990	1.104	0.114
C(20)-C(19)	1.394(5)	1.399	0.005	C(29)-C(28)	1.513(5)	1.527	0.014
C(11)-C(12)	1.400(5)	1.396	−0.004	C(5)-H(5)	0.950	1.082	0.132
C(11)-C(10)	1.396(5)	1.405	0.009	C(5)-C(4)	1.382(6)	1.390	0.008
C(19)-C(18)	1.388(5)	1.395	0.007	C(14)-H(14)	0.950	1.083	0.133
C(19)-C(24)	1.522(5)	1.513	−0.009	C(23)-H(23A)	0.980	1.094	0.114
C(16)-C(17)	1.479(5)	1.472	−0.007	C(23)-H(23B)	0.980	1.095	0.115
C(6)-C(7)	1.521(5)	1.515	−0.006	C(23)-H(23C)	0.980	1.089	0.109
C(6)-C(1)	1.390(5)	1.396	0.006	C(28)-H(28A)	0.990	1.094	0.104
C(6)-C(5)	1.387(5)	1.393	0.006	C(28)-H(28B)	0.990	1.092	0.102
C(17)-C(18)	1.376(5)	1.389	0.013	C(2)-H(2)	0.950	1.082	0.132
C(17)-C(22)	1.396(5)	1.403	0.007	C(2)-C(3)	1.382(6)	1.389	0.007
C(18)-H(18)	0.950	1.083	0.133	C(3)-H(3A)	0.950	1.083	0.133
C(22)-H(22)	0.950	1.081	0.131	C(3)-C(4)	1.372(6)	1.389	0.017
C(9)-C(10)	1.483(5)	1.483	0.000	C(4)-H(4A)	0.950	1.083	0.133
Bond angle [°]	**Exp. [a]**	**Calcd. [b]**	**Difference**	**Bond angle [°]**	**Exp. [a]**	**Calcd. [b]**	**Difference**
C(21)-O(2)-C(23)	117.2(3)	118.3	1.1	C(26)-C(25)-H(25A)	109.7	110.3	0.6
C(20)-O(3)-H(3)	109.5	106.3	−3.2	C(26)-C(25)-H(25B)	109.7	110.0	0.3
C(27)-O(4)-H(4)	109.5	109.0	−0.5	C(6)-C(1)-Cl(1)	118.6(3)	119.7	1.1
C(8)-N(4)-C(11)	121.5(3)	121.4	−0.1	C(2)-C(1)-Cl(1)	118.8(3)	118.1	−0.7
C(8)-N(4)-C(16)	104.0(3)	103.3	−0.7	C(2)-C(1)-C(6)	122.6(4)	122.2	−0.4
C(16)-N(4)-C(11)	134.5(3)	135.0	−0.5	N(5)-C(24)-C(19)	112.0(3)	113.4	1.4
C(8)-N(1)-C(9)	121.1(3)	121.8	0.7	N(5)-C(24)-H(24A)	109.2	111.3	2.1
C(8)-N(1)-C(7)	118.2(3)	118.5	0.3	N(5)-C(24)-H(24B)	109.2	106.6	−2.6
C(9)-N(1)-C(7)	120.7(3)	119.6	−1.1	C(19)-C(24)-H(24A)	109.2	109.6	0.4
C(25)-N(5)-C(24)	112.4(3)	111.9	−0.5	C(19)-C(24)-H(24B)	109.2	108.9	−0.3
C(25)-N(5)-C(29)	109.6(3)	111.0	1.4	H(24A)-C(24)-H(24B)	107.9	106.8	−1.1
C(29)-N(5)-C(24)	112.6(3)	111.5	−1.1	C(25)-C(26)-H(26A)	109.3	109.1	−0.2
C(8)-N(2)-N(3)	104.9(3)	106.3	1.4	C(25)-C(26)-H(26B)	109.3	109.9	0.6
C(16)-N(3)-N(2)	109.4(3)	109.3	−0.1	H(26A)-C(26)-H(26B)	108.0	107.5	−0.5
N(4)-C(8)-N(1)	121.9(3)	121.5	−0.4	C(27)-C(26)-C(25)	111.4(3)	110.9	−0.5
N(2)-C(8)-N(4)	112.6(3)	112.0	−0.6	C(27)-C(26)-H(26A)	109.3	110.5	1.2
N(2)-C(8)-N(1)	125.5(3)	126.4	0.9	C(27)-C(26)-H(26B)	109.3	108.8	−0.5
O(2)-C(21)-C(20)	115.4(3)	115.4	0.0	C(10)-C(15)-H(15)	119.8	117.6	−2.2
O(2)-C(21)-C(22)	124.4(3)	124.9	0.5	C(10)-C(15)-C(14)	120.4(4)	120.6	0.2
C(22)-C(21)-C(20)	120.2(3)	119.7	−0.5	C(14)-C(15)-H(15)	119.8	121.7	1.9
O(3)-C(20)-C(21)	117.4(3)	118.2	0.8	O(4)-C(27)-C(26)	111.8(3)	112.6	0.8
O(3)-C(20)-C(19)	122.7(3)	122.1	−0.6	O(4)-C(27)-H(27)	108.9	109.4	0.5
C(19)-C(20)-C(21)	119.9(3)	119.8	−0.1	O(4)-C(27)-C(28)	106.8(3)	107.3	0.5
C(12)-C(11)-N(4)	123.0(3)	123.3	0.3	C(26)-C(27)-H(27)	108.9	108.8	−0.1
C(10)-C(11)-N(4)	117.1(3)	116.7	−0.4	C(28)-C(27)-C(26)	111.4(3)	111.0	−0.4
C(10)-C(11)-C(12)	119.8(4)	119.9	0.1	C(28)-C(27)-H(27)	108.9	108.7	−0.2
C(20)-C(19)-C(24)	120.5(3)	119.8	−0.7	C(12)-C(13)-H(13)	119.7	118.9	−0.8
C(18)-C(19)-C(20)	118.8(3)	120.5	1.7	C(12)-C(13)-C(14)	120.7(4)	121.1	0.4
C(18)-C(19)-C(24)	120.6(3)	119.6	−1.0	C(14)-C(13)-H(13)	119.7	120.0	0.3
N(4)-C(16)-C(17)	126.8(3)	127.2	0.4	N(5)-C(29)-H(29A)	109.8	110.2	0.4
N(3)-C(16)-N(4)	109.1(3)	109.1	0.0	N(5)-C(29)-H(29B)	109.8	108.2	−1.6
N(3)-C(16)-C(17)	124.0(3)	123.7	−0.3	N(5)-C(29)-C(28)	109.3(3)	111.4	2.1
C(1)-C(6)-C(7)	120.6(3)	119.9	−0.7	H(29A)-C(29)-H(29B)	108.3	107.1	−1.2
C(5)-C(6)-C(7)	122.6(3)	122.9	0.3	C(28)-C(29)-H(29A)	109.8	111.0	1.2
C(5)-C(6)-C(1)	116.7(4)	117.2	0.5	C(28)-C(29)-H(29B)	109.8	109.9	0.1
C(18)-C(17)-C(16)	119.7(3)	119.6	−0.1	C(6)-C(5)-H(5)	119.4	119.1	−0.3

(*continued on next page*)

Table 4 (*continued*)

Bond Distances (Å)	Exp.[a]	Calcd.[b]	Difference	Bond Distances (Å)	Exp. [a]	Calcd. [b]	Difference
C(18)-C(17)-C(22)	119.8(3)	119.3	−0.5	C(4)-C(5)-C(6)	121.2(4)	121.5	0.3
C(22)-C(17)-C(16)	120.4(3)	121.0	−0.4	C(4)-C(5)-H(5)	119.4	119.3	−0.1
C(19)-C(18)-H(18)	119.2	119.7	0.5	C(15)-C(14)-H(14)	120.1	120.3	0.2
C(17)-C(18)-C(19)	121.6(4)	121.0	−0.6	C(13)-C(14)-C(15)	119.7(4)	119.4	−0.3
C(17)-C(18)-H(18)	119.2	119.4	0.2	C(13)-C(14)-H(14)	120.1	120.3	0.2
C(21)-C(22)-C(17)	119.6(3)	120.6	1.0	O(2)-C(23)-H(23A)	109.5	105.8	−3.7
C(21)-C(22)-H(22)	120.2	120.0	−0.2	O(2)-C(23)-H(23B)	109.5	111.5	2.0
C(17)-C(22)-H(22)	120.2	119.3	−0.9	O(2)-C(23)-H(23C)	109.5	111.4	1.9
O(1)-C(9)-N(1)	120.5(3)	121.3	0.8	H(23A)-C(23)-H(23B)	109.5	109.3	−0.2
O(1)-C(9)-C(10)	123.4(4)	123.2	−0.2	H(23A)-C(23)-H(23C)	109.5	109.4	−0.1
N(1)-C(9)-C(10)	116.1(3)	115.5	−0.6	H(23B)-C(23)-H(23C)	109.5	109.4	−0.1
C(11)-C(12)-H(12)	120.1	120.4	0.3	C(27)-C(28)-C(29)	112.1(3)	111.2	−0.9
C(13)-C(12)-C(11)	119.8(4)	119.5	−0.3	C(27)-C(28)-H(28A)	109.2	108.6	−0.6
C(13)-C(12)-H(12)	120.1	120.1	0.0	C(27)-C(28)-H(28B)	109.2	109.9	0.7
C(11)-C(10)-C(9)	121.7(3)	122.3	0.6	C(29)-C(28)-H(28A)	109.2	109.9	0.7
C(15)-C(10)-C(11)	119.5(3)	119.5	0.0	C(29)-C(28)-H(28B)	109.2	109.8	0.6
C(15)-C(10)-C(9)	118.7(3)	118.1	−0.6	H(28A)-C(28)-H(28B)	107.9	107.4	−0.5
N(1)-C(7)-C(6)	112.6(3)	114.6	2.0	C(1)-C(2)-H(2)	120.4	119.6	−0.8
N(1)-C(7)-H(7A)	109.1	107.3	−1.8	C(1)-C(2)-C(3)	119.2(4)	119.4	0.2
N(1)-C(7)-H(7B)	109.1	106.6	−2.5	C(3)-C(2)-H(2)	120.4	121.0	0.6
C(6)-C(7)-H(7A)	109.1	109.7	0.6	C(2)-C(3)-H(3)	120.3	119.7	−0.6
C(6)-C(7)-H(7B)	109.1	109.6	0.5	C(4)-C(3)-C(2)	119.4(4)	119.7	0.3
H(7A)-C(7)-H(7B)	107.8	108.7	0.9	C(4)-C(3)-H(3)	120.3	120.6	0.3
N(5)-C(25)-H(25A)	109.7	108.5	−1.2	C(5)-C(4)-H(4)	119.6	119.7	0.1
N(5)-C(25)-H(25B)	109.7	109.9	0.2	C(3)-C(4)-C(5)	120.9(4)	120.0	−0.9
N(5)-C(25)-C(26)	109.6(3)	111.0	0.4	C(3)-C(4)-H(4)	119.6	120.3	0.7
H(25A)-C(25)-H(25B)	108.2	107.0	−1.2				

a: Experimental geometry parameters for molecule **1**;.
b: Calculated geometry parameters for conformer **1–1**.

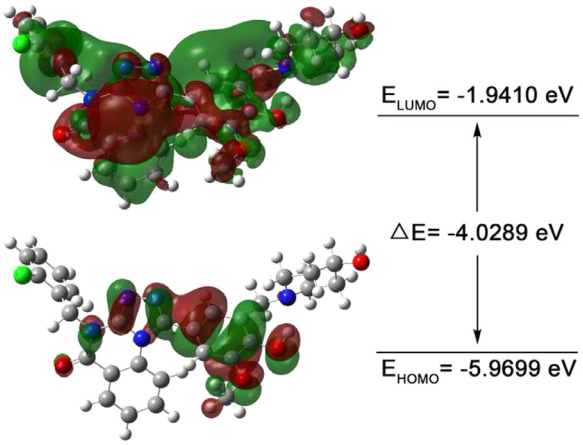

Fig. 6. The HOMO and LUMO of conformer **1–1**.

E_{LUMO} = 1.9410 eV and I = -E_{HOMO} = 5.9699 eV. The chemical potential and global hardness are given by using the relation μ = -(I + A)/2 = −3.9555 eV, η = (I-A)/2 = 2.0145 eV and electrophilicity index (ω) = $\mu^2/2\eta$ = 3.8832 eV.

4.6. Vibrational assignment

Based on the characteristic vibrations of –OH, C–H, $C = O$, $C = C$ and C–Cl, the vibrational analysis of **1** was carried out. The title molecule **1** has 67 atoms in total, so the normal vibration mode is 3*n - 6 = 195. The theoretical wavenumbers are higher than the experimental wavenumbers, since non-harmonic vibrations were ignored [42]. The theoretical errors were corrected using a scaling factor of 0.961 for B3LYP. The experimental wavenumbers were recorded in the region of 4000 – 400 cm^{-1} using Bruker IFS-55 V IR spectrometer. As shown in Fig.S4.

4.6.1. –OH vibration

The –OH vibrations are expected in the region of 3500 – 3100 cm^{-1} [43]. For **1**, the –OH vibration was observed at 3355.05 cm^{-1}.

4.6.2. C–H vibration

The C–H asymmetric stretch vibrations frequencies of the methyl group and methylene group are expected in the region of 3009 – 2908 cm^{-1} [44]. The out-of-plane bending vibrations of the substituted benzene rings C–H are expected in the region of 900 – 730 cm^{-1}. For, the methyl and methylene group's C–H stretching mode were observed at 2941.39 cm^{-1}, and the out-of-plane bending vibration of Ar–H was observed at 759.33 cm^{-1}.

4.6.3. C = O vibration

The $C = O$ stretching vibrations are expected in the region of 1870 – 1540 cm^{-1} [45]. For **1**, the $C = O$ vibration was observed at 1684.52 cm^{-1}.

4.6.4. C = C vibration

The $C = C$ stretching vibrations of the substituted benzene ring are expected in the region of 1620 – 1450 cm^{-1} [29]. For **1**, the aromatic $C = C$ vibrations are observed at 1613.16 cm^{-1}, 1597.74 cm^{-1}, 1563.99 cm^{-1}, 1496.01 cm^{-1} and 1470.46 cm^{-1}.

3.6.5. C–Cl vibration

The C–Cl stretching vibrations are expected in the region of 760 – 505 cm^{-1} [46]. The C–Cl absorption frequencies may appear to shift because of the vibrational coupling with the neighboring C group. For **1**, the C–Cl vibration was observed at 683.16 cm^{-1}.

4.7. ^{13}C NMR spectral analysis

NMR spectroscopy is widely used to confirm the structure of the compound [47–49]. For **1**, the theoretical ^{13}C NMR chemical shifts were calculated using the DFT/GIAO method [30], and the experimental spectrum was recorded on a Bruker ACF-400 spectrometer. The calculated and experimental ^{13}C NMR chemical shifts

Table 5
Calculated and experimental ^{13}C chemical shifts (ppm) of **1**.

Assignments	Calc.	Exp.
C9	164.75	158.88
C20	157.06	149.17
C16	156.32	148.89
C8	154.28	148.69
C21	153.56	148.20
C1	144.67	135.04
C11	141.37	134.65
C13	139.55	133.43
C6	138.83	132.20
C15	134.69	129.80
C2	134.39	129.73
C3	132.80	129.39
C4	131.30	127.86
C14	131.09	127.79
C19	130.13	127.10
C5	129.24	123.98
C18	127.16	123.13
C17	125.85	118.40
C10	122.80	117.69
C12	121.26	116.29
C22	114.48	112.86
C27	73.50	65.91
C24	62.22	59.03
C23	56.15	56.41
C29	55.61	50.68
C25	51.79	50.68
C7	47.66	44.25
C26	38.83	34.64
C28	36.66	34.64

Numbering is according to Fig. 2.

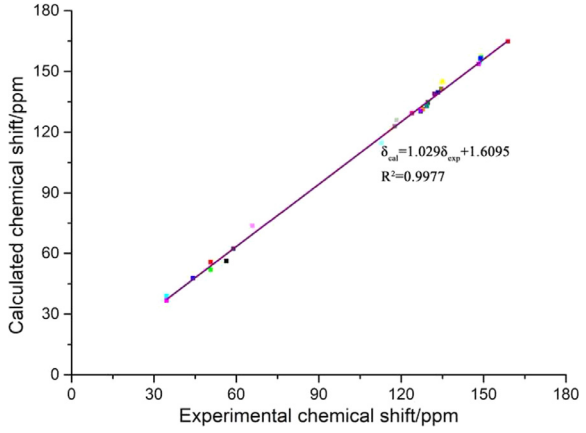

Fig. 7. Linear relationship between calculated and experimental ^{13}C NMR chemical shift of **1**.

of **1** were listed in Table 5. Different hybrid degree of carbon atom will cause different chemical shift [29]. The conjugation action can lead to an increase in the chemical shifts of carbon atom [49]. For **1**, the C atoms' calculated chemical shifts attached to the N, O and Cl heteroatoms are in the region of 164.75 – 47.66 ppm. Furthermore, the calculated chemical shifts of aromatic and aliphatic C atoms are in the region of 157.06 – 114.48 ppm and 73.50 – 36.66 ppm, respectively.

The linear correlations between calculated and experimental data of ^{13}C NMR spectrum were meaned with the equation: $\delta_{cal} = 1.029\delta_{exp} + 1.6095$ (correlation coefficient $R^2 = 0.9977$). We can observe good correlations between the calculated and experimental chemical shifts, as shown in Fig. 7.

4.8. Molecular docking analysis

Molecular docking plays a vital role in computer-aided drug design and the development of new chemotherapeutic drugs [50,51]. Molecular docking aims to understand the interaction mechanisms between ligand molecules and target proteins by analyzing various structural parameters, and find out the binding sites and optimized conformations of ligand molecules with proteins [52–54]. Docking of reference compound (**SHP244**) and **1** with SHP2 protein were carried out using the Surflex-Dock (SFXC) docking mode in the SYBYL-X 2.0 software [55,56], to understand the mode of interaction and binding site position. The docking interactions between **SHP244** and **1** with SHP2 protein were compared, as shown in Table 6.

The docking scores of **SHP244** and **1** with SHP2 protein were 8.30 and 7.43, respectively. **SHP244** and **1** bound to residues R265, Q269 and Q79 of SHP2 protein; **SHP244** bound to residue L262, and compound **1** also bound to residue K266 of the same protein, as shown in Fig. 8. The docking structure was different from the crystal structure and DFT-optimized 1–1 conformation, which may be caused by the interaction between **1** and the amino acid residues of SHP2. For **SHP244** and **1**, the N-2 atom of the triazole ring formed a hydrogen bond with residue R265, the N-3 atom of the triazole ring formed a hydrogen bond with residue Q269. For **SHP244**, the O atom of the phenolic hydroxyl group formed a hydrogen bond with residues Q79, L262 and R265, and the O atom of the methoxy group was combined with residue Q79 through hydrogen bonding mediated by a water molecule (H_2O 899). For **1**, the N-2 atom of the triazole ring also formed a hydrogen bond with residue Q269, the N-3 atom of the triazole ring also formed a hydrogen bond with residue R265, and the O atoms of the methoxy and hydroxypiperidine rings form hydrogen bonds with residues K266 and Q79, respectively. In summary, compound **1** not only retains the original main amino acid residues that can form hydrogen bonds with the SHP2 protein, but also adds the amino acid residue K266.

4.9. Molecular dynamics analysis

We further ran MD simulation based on docked data to verify the results of molecular docking. In order to evaluate the dynamic stability of the **1**-SHP2 complex, the time dependence of the root mean square deviation (RMSD) of the MD simulation for all atomic position of the **1**-SHP2 complex relative to those of the initial structures are studied. The MD trajectory of SHP2 protein, sharply to 19.38 Å within 100 ps then averages at 20.97 Å after 200 ps, as shown in Fig. 9. For **1**-SHP2 complex rises, sharply to 19.36 Å within 100 ps then averages at 21.13 Å after 200 ps.

We also further used MD to simulate the interaction between SHP2 protein and compound **1**, as shown in Fig. 10. In the triazole ring of compound **1**, the N-2 atom formed a hydrogen bond with the residue R265, and the N-4 atom formed a hydrogen bond with the residues R265 and K266, respectively. The N-4 atom of the triazole ring formed an electrostatic interaction with the residue Q79, and the Cl atom also formed an electrostatic interaction with the residue K266. The triazole ring formed Pi–cation interactions with residues R265 and K266, respectively; in addition, the benzene ring and ketone ring of quinazolinone also formed Pi–cation interactions with residue K266.

4.10. SHP2 enzyme inhibitory activity

The SHP2 enzyme inhibitory activity of **1** was evaluated at 10 μM, **SHP244** (SHP2 inhibitor) [11] was used as a reference compound. The SHP2 enzyme inhibitory activity of **1** (inhibition rate: 23.33%) is better than **SHP244** (19.67%).

Table 6
Docking scoring results and hydrogen bondings of compounds with SHP2 protein.

Compound	PDB	Total Score	Hydrogen-bonding residues	Number of Hydrogen-bonding
SHP244	6BMR	8.30	Q79/R265/Q269/L262	7
1	6BMR	7.43	Q79/R265/Q269/K266	7

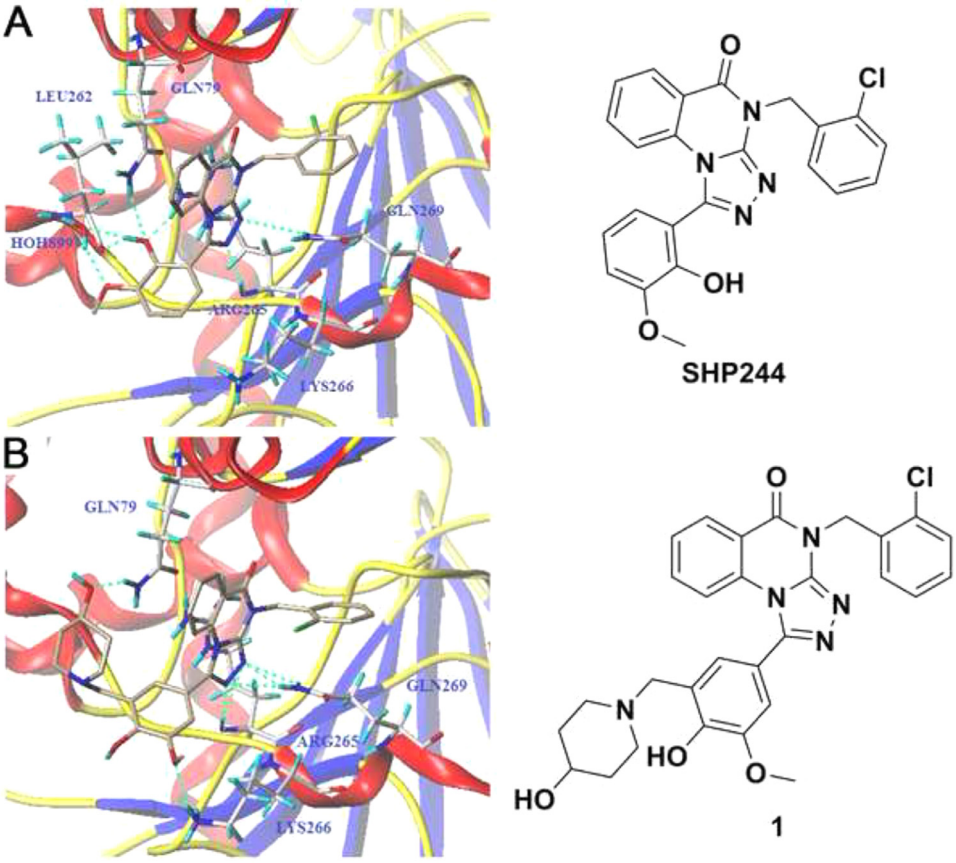

Fig. 8. Docking diagram of **SHP244** (A) and **1** (B) with SHP2 protein (PDB: 6BMR), (hydrogen bond: light blue dashed line).

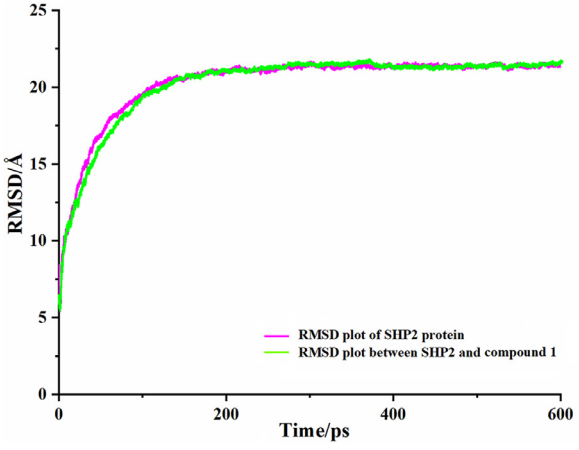

Fig. 9. RMSD plots for the simulation of **1**-**SHP2**.

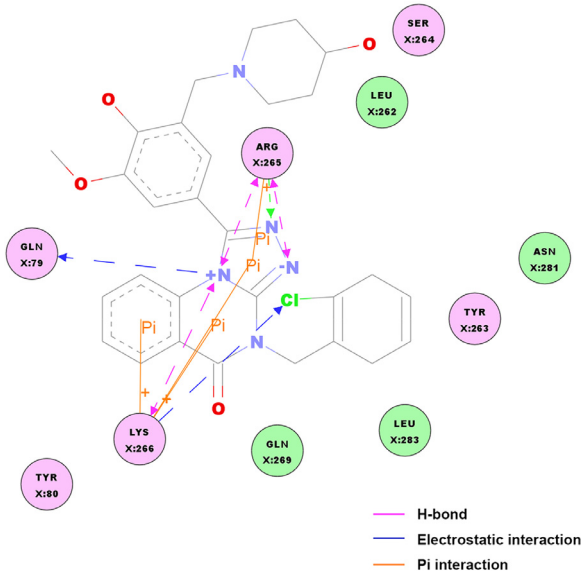

Fig. 10. MD simulation diagram of the interaction between compound **1** and SHP2 protein (PDB: 6BMR).

5. Conclusions

In this study, 4-(2-chlorobenzyl)−1-(4–hydroxy-3-((4-hydroxypiperidin-1-yl)methyl)−5- methoxyphenyl)-[1,2,4] triazolo[4,3-*a*]quinazolin-5(4H)-one (**1**) was synthesised for the first time. The structural properties of **1** were explored by spectroscopy (^{1}H NMR, ^{13}C NMR, MS and FT-IR) and X-ray crystallography method. The crystal structure determined by X-ray diffraction were consistent with the optimized structure determined by DFT using the B3LYP/6–311 G (2d, p) method. The molecular surfaces were described by molecular electrostatic potential (MEP). The chemical reactivity of the molecule was calculated from frontier molecular orbitals (FMOs) energy data. The theoretical and experimental vibrational spectra (FT-IR) were used to confirm the functional groups. The calculated and experimental ^{13}C NMR chemical shifts have a good correlation. The docking result of **1** with SHP2 protein showed that compound **1** not only retains the original main amino acid residues (Q79, R265 and Q269) that can form hydrogen bonds with the SHP2 protein, but also adds the amino acid residue K266. The MD simulation results shown that there are hydrogen bonds, electrostatic interactions and Pi interactions between compound **1** and SHP2 proteins. The inhibitory activity of **1** on SHP2 protein at 10 μM is better than the reference compound (**SHP244**).

Declaration of Competing Interest

The authors declare that they have no known competing financial interests or personal relationships that could have appeared to influence the work reported in this paper.

CRediT authorship contribution statement

Qingmei Wu: Writing – original draft, Data curation, Methodology, Writing – review & editing. **Zhaopeng Zheng:** Software, Data curation, Writing – review & editing. **Wenjun Ye:** Writing – review & editing. **Qian Guo:** Writing – review & editing. **Tianhui Liao:** Writing – review & editing. **Di Yang:** Writing – review & editing. **Chunshen Zhao:** Writing – review & editing. **Weike Liao:** Writing – review & editing. **Huifang Chai:** Supervision, Writing – review & editing. **Zhixu Zhou:** Supervision, Software, Writing – review & editing.

Acknowledgments

We want to thank the Guizhou Provincial Natural Science Foundation ([2020]1Y393), the Science and Technology Fund of Guizhou Provincial Health Department (gzwjkj2020–1–238) and the Guizhou University of Traditional Chinese Medicine 2018 annual academic new seedling cultivation and innovation exploration special project cultivation project plan (Qiankehe platform talent [2018]5766–14) for financial support.

Supplementary materials

Supplementary material associated with this article can be found, in the online version, at doi:10.1016/j.molstruc.2021.131367.

References

[1] Y. Ali, S.A. Hamid, U. Rashid, Biomedical applications of aromatic azo aompounds, Mini-Rev. Med. Chem. 18 (2018) 1548–1558.
[2] M.R. Maliyappa, J. Keshavayya, N.M. Mallikarjuna, P.M. Krishna, N. Shivakumara, T. Sandeep, K. Sailaja, M.A. Nazrulla, Synthesis, haracterization, pharmacological and computational studies of 4,5,6, 7-tetrahydro-1, 3-benzothiazole incorporated azo dyes, J. Mol. Struct. 1179 (2019) 630–641.
[3] W. Geoffrey, D.B. Tracey, D. Patrizia, S. Angela, S. Dong-Fang, D. Andrew, M.F. Westwell, G. Stevens, Antitumour benzothiazoles. Part 10: the synthesis and antitumour activity of enzothiazole substituted quinol derivatives, Bioorg. Med. Chem. Lett. 10 (2000) 513–515.
[4] J. Sahoo, S.K. Paidesetty, Medicinal interest of azogbased organic compounds: a review, Asian J. Pharm. Clin. Res. 9 (2016) 33–39.
[5] S. Prakash, G. Somiya, N. Elavarasan, K. Subashini, S. Kanaga, R. Dhandapani, M. Sivanandam, P. Kumaradhas, C. Thirunavukkarasu, V. Sujatha, Synthesis and characterization of novel bioactive azo compounds fused with benzothiazole and their versatile biological applications, J. Mol. Struct. 1224 (2021) 129016.
[6] V. Alagarsamy, M. Rupeshkumar, K. Kavitha, S. Meena, D. Shankar, A.A. Siddiqui, R. Rajesh, Synthesis and pharmacological investigation of novel 4-(2-methylphenyl)-1-substituted-4H-[1,2,4]triazolo[4,3-*a*]quinazolin -5-ones as new class of H1-antihistaminic agents, Eur. J. Med. Chem. 43 (2008) 2331–2337.
[7] M. Gobinath, N. Subramanian, V. Alagarsamy, Design, synthesis and H1-antihistaminic activity of novel 1-substituted-4-(3-chlorophenyl)-[1,2,4] triazolo [4,3-a] quinazolin-5(4H)-ones, J. Saudi Chem. Soc. 19 (2015) 282–286.
[8] M. Gobinath, N. Subramanian, V. Alagarsamy, S. Nivedhitha, V.R. Solomon, Design and synthesis of 1-substituted-4-(4-nitrophenyl)-[1,2,4]triazolo[4,3-*a*]quinazolin-5(4H)-ones as a new class of antihistaminic agents, Russ. J. Bioorg. Chem. 46 (2020) 403–408.
[9] V. Alagarsamy, V.R. Solomon, M. Murugan, Synthesis and pharmacological investigation of novel 4-benzyl-1-substituted-4H-[1,2,4]triazolo[4,3-*a*]quinazolin-5-ones as new class of H1-antihistaminic agents, Bioorg. Med. Chem. 15 (2007) 4009–4015.
[10] N.M. Abdel Gawad, H.H. Georgey, R.M. Youssef, N.A. El Sayed, Design, synthesis, and anticonvulsant activity of novel quinazolinone analogues, Med. Chem. Res. 20 (2010) 1280–1286.
[11] M. Fodor, E. Price, P. Wang, H.Y. Lu, A. Argintaru, Z.L. Chen, H.X.Hao M.Glick, M. Kato, R. Koenig, J.R. LaRochelle, G. Liu, E. McNeill, D. Majumdar, G.A. Nishiguchi, L.B. Perez, G. Paris, C.M. Quinn, T. Ramsey, M. Sendzik, M.D. Shultz, S.L. Williams, T. Stams, S.C. Blacklow, M.G. Acker, M.J. LaMarche, Dual allosteric inhibition of SHP2 phosphatase, ACS Chem. Biol. 13 (2018) 647–656.
[12] S. Danylchenko, O. Drushlyak, S. Kovalenko, S. Kovalenko, A. Elliott, J. Zuegg, Primary antimicrobial screening of novel [1,2,4]triazolo[4,3 -*a*]quinazolin-5(4H)-one derivatives, Science Rise 4 (2016) 59–64.
[13] A.A. El-Tombary, K.A. Ismail, O.M. Aboulwafa, A. Mohsen, M.E. Omar, M.Z. El-Azzouni, S.T. El-Mansoury, Novel triazolo[4, 3-*a*]quinazolinone and bis–triazolo [4, 3-a:4, 3′-c]quinazolines: synthesis and antitoxoplasmosis effect, Farmaco 54 (1999) 486–495.
[14] M. Driowya, J. Leclercq, V. Verones, A. Barczyk, M. Lecoeur, N. Renault, N. Flouquet, A. Ghinet, P. Berthelot, N. Lebegue, Synthesis of triazoloquinazolinone based compounds as tubulin polymerization inhibitors and vascular disrupting agents, Eur. J. Med. Chem. 115 (2016) 393–405.
[15] B.G. Neel, H. Gu, L. Pao, The 'Shp'ing News: SH2 Domain-Containing Tyrosine Phosphatases in Cell Signaling, Trends Biochem. Sci. 28 (2003) 284–293.
[16] R.J. Chan, G.S. Feng, Ptpn11 is the First Identified Proto-Oncogene That Encodes a Tyrosine Phosphatase, Blood 109 (2007) 862–867.
[17] T. Tiganis, A.M. Bennett, Protein Tyrosine Phosphatase Function: the Substrated Perspective, Biochem. J. 402 (2007) 1–15.
[18] J. Li, H.-.B. Jie, Y. Lei, N. Gildener-Leapman, S. Trivedi, PD-1/SHP-2 Inhibits Tc1/Th1 Phenotypic Responses and the Activation of T Cells in the Tumor Microenvironment, Cancer Res 75 (2015) 508–518.
[19] M. Tartaglia, E.L. Mehler, R. Godberg, G. Zampino, H.G. Brunner, H. Kremer, I. Van Der Burgt, A.H. Crosby, A. Ion, S. Jeffery, K. Kalidas, J.A. Patton, R.S. Kucherlapati, B.D. Gelb, Mutations in Ptpn11, Encoding the Protein Tyrosine Phosphatase SHP-2, Cause Noonan syndrome, Nat. Genet. 29 (2001) 465–468.
[20] M. Tartaglia, C.M. Niemeyer, A. Fragale, X. Song, J. Buechner, A. Jung, K. Hählen, H. Hasle, J.D. Licht, B.D. Gelb, Somatic Mutations in Ptpn11 in Juvenile Myelomonocytic Leukemia, Myelodysplactic Syndromes and Acute Myeloid Leukemia, Nat. Genet. 34 (2003) 148–150.
[21] S. Mulero-Navarro, A. Sevilla, A.C. Roman, D.-F. Lee, S.L. D'Souza, S. Pardo, I. Riess, J. Su, N. Cohen, C. Schaniel, N.A. Rodriguez, A. Baccarini, B.D. Brown, A. Cavé, M. Strullu, S. Yalcin, C.Y. Park, P.S. Dhandapany, G. Yongchao, L. Edelmann, S. Bahieg, P. Raynal, E. Flex, M. Tartaglia, K.A. Moore, I.R. Lemishka, B.D. Gelb, Myleoid Dysregulation in a Human Induced Pluripotent Stem Cell Model of Ptpn11-Associated Juvenile Myleomonocytic Leukemia, Cell Rep 13 (2015) 504–515.
[22] M. Bentires-Alj, J.G. Paez, F.S. David, H. Keilhack, B. Halmos, K. Naoki, J.M. Maris, A. Richardson, A. Bardelli, D.J. Sugarbaker, W.G. Richards, J. Du, L. Girard, J.D. Minna, M.L. Loh, D.E. Fisher, V.E. Velculescu, B. Vogelstein, M. Meyerson, W.R. Sellers, B.G. Neel, Activating Mutations of the Noonan Syndrome-Associated SHP2/Ptpn11 Gene in Human Solid Tumors and Adult Acute MyelogenousLeukemia, Cancer Res 64 (2004) 8816–8820.
[23] D. Miyamoto, M. Miyamoto, A. Takahashi, Y. Yomogita, H. Hagashi, S. Kondo, M. Hatakeyama, Isolation of a Distinct Class of Gain-of-Function SHP-2 mutants with Oncogenic RAS-like Transforming Activity From Solid Tumors, Oncogene 27 (2008) 3508–3515.
[24] R.A. Costa, P.O. Pitt, M.L.B. Pinheiro, K.M.T. Oliveira, K.S. Salomé, A. Barison, E.V. Costa, Spectroscopic investigation, vibrational assignments, HOMO-LUMO, NBO, MEP analysis and molecular docking studies of oxoaporphine alkaloid liriodenine, Spectrochim, Acta A Mol.Biomol. Spectrosc 174 (2017) 94–104.

[25] Y. Leblanc, W.C. Black, C.C. Chan, S. Charleson, D. Delorme, D. Denis, J.Y. Gauthier, E.L. Grimm, R. Gordon, D. Guay, P. Hamel, S. Kargman, C.K. Lau, J. Mancini, M. Ouellet, D. Percival, P. Roy, K. Skorey, P. Tagari, P. Vickers, E. Wong, L. Xu, P. Prasit, Synthesis and biological evaluation of both enantiomers of L-761,000 as inhibitors of cyclooxygenase 1 and 2, Bioorg. Med. Chem. Lett. 6 (1996) 731–736.
[26] A.V. Ivachtchenko, P.M. Yamanushkin, O.D. Mitkin, Bromination of indomethacin, Mendeleev Commun 20 (2010) 111–112.
[27] A.V. Ivashchenko, P.M. Yamanushkin, O.D. Mit'Kin, Synthesis and antiviral activity of functionally substituted indole-3-acetic acids, Pharm. Chem. J. 45 (2011) 261–266.
[28] Y-N.P. Chen, M.J. LaMarche, H.M. Chan, P. Fekkes, J. Garcia-Fortanet, M.G. Acker, B. Antonakos, C.H. Chen, Z. Chen, V.G. Cooke, J.R. Dobson, Z. Deng, F. Fei, B. Firestone, M. Fodor, C. Fridrich, H. Gao, D. Grunenfelder, H.X. Hao, J. Jacob, S. Ho, K. Hsiao, Z.B. Kang, R. Karki, M. Kato, J. Larrow, L.R. La Bonte, F. Lenoir, G. Liu, S. Liu, D. Majumdar, M.J. Meyer, M. Palermo, L. Perez, M. Pu, E. Price, C. Quinn, S. Shakya, M.D. Shultz, J. Slisz, K. Venkatesan, P. Wang, M. Warmuth, S. Williams, G. Yang, J. Yuan, J.H. Zhang, P. Zhu, T. Ramsey, N.J. Keen, W.R. Sellers, T. Stams, P.D. Fortin, Allosteric inhibition of SHP2 phosphatase inhibits cancers driven by receptor tyrosine kinases, Nature 535 (2016) 148–152.
[29] Q.M. Wu, Y.M. Chen, D.M. Chen, Z.X. Zhou, Synthesis, crystal structure and vibrational properties studies of 2-((4-(4,4,5,5-tetramethyl-1,3,2-dioxaborolan-2-yl)phenoxy)methyl)benzonitrile and N-(3-bromobenzyl)-4- (4,4,5,5-tetramethyl-1,3,2-dioxaborolan-2-yl)aniline, J. Mol. Struct 1229 (2021) 129782.
[30] R. Ditchfield, Self-consistent perturbation theory of diamagnetism. I. A gageinvariant LCAO (linear combination of atomic orbitals) method for NMR chemical shifts, Mol. Phys. 27 (1974) 714–722.
[31] Tripos International Sybyl-X 2.0, Tripos International, St. Louis, MO. USA (2012).
[32] D.A. Case, R. Anandakrishnan, K. Ayers, R. Betz, Y.J. Bomble, R.A. Brown, S. Brozell, Q.Cai, D.S.Cerutti, T.E.C. Iii, (2012).
[33] Y. Liu, Y.L. Zhao, Q. Ren, Z.X. Zhou, H.F. Chai, C.S. Zhao, Synthesis, crystal structure and DFT study of a novel planar bipyridyl compound 6,6'-bis(trifluoromethyl)-3,3'-bipyridine, J. Mol. Struct. 1208 (2020) 127869.
[34] M. Kwit, N.D. Sharma, D.R. Boyd, J. Gawronski, Determination of absolute configuration of conformationally flexible cis-dihydrodiol metabolites: effect of diene substitution pattern on the circular dichroism spectra and optical rotations, Chirality 20 (2008) 609–620.
[35] N. Kanagathara, F. MaryAnjalin, V. Ragavendran, D. Dhanasekaran, R. Usha, R. Gowri Shankar Rao, M.K. Marchewka, Experimental and theoretical (DFT) investigation of crystallographic, spectroscopic and Hirshfeld surface analysis of anilinium arsenate, J. Mol. Struct. 1223 (2020) 128965.
[36] P. Zhou, W.Y. Qiu, S.B. Liu, N.Z. Jin, Halogen as halogen-bonding donor and hydrogen-bonding acceptor simultaneously in ring-shaped H3N·X(Y)·HF (X = Cl, Br and Y = F, Cl, Br) complexes, Phys. Chem. Chem. Phys 13 (2011) 7408–7418.
[37] C.K. Atay, T. Tilki, B. Dede, Design and synthesis of novel ribofuranose nucleoside analogues as antiproliferative agents: a molecular docking and DFT study, J. Mol. Liq. 269 (2018) 315–326.
[38] H.H. Greenwood, Molecular orbital theory of reactivity in aromatic hydrocarbons, J. Chem. Phys. 20 (1952) 1653–1653.
[39] M.D. Rozeboom, I.M. Tegmo-Larsson, K.N. Houk, Frontier molecular orbital theory of substitutent effects on regioselectivities of nucleophilic additions and cycloadditions to benzoquinones and naphthoquinones, J. Org. Chem. 46 (1981) 2338–2345.
[40] F. Perveen, N. Arshad, R. Qureshi, J. Nowsherwan, A. Sultan, B. Nosheen, H. Rafique, Electrochemical, spectroscopic and theoretical monitoring of anthracyclines' interactions with DNA and ascorbic acid by adopting two routes: cancer cell line studies, PLoS ONE 13 (2018) e0205764.
[41] N. Arshad, M. Rafiq, R. Ujan, A. Saeed, S.I. Farooqi, F. Perveen, P.A. Channar, S. Ashraf, Q. Abbas, A. Ahmed, T. Hokelek, M. Kaur, J.P. Jasinski, Synthesis, X-ray crystal structure elucidation and Hirshfeld surface analysis of N-((4-(1H-benzo[*d*]imidazole-2-yl)phenyl)carbamothioyl)benzamide: investigations for elastase inhibition, antioxidant and DNA binding potentials for biological applications, RSC Adv. 10 (2020) 20837.
[42] N.T. Abdel Ghani, A.M. Mansour, 2-[(1H-B*enzimidazol*-2-*ylmethyl*)-*amino*]-benzoic acid methyl ester: crystal structure, DFT calculations and biological activity evaluation, Spectrochim, Acta A Mol.Biomol. Spectrosc 81 (2011) 754–763.
[43] J. Li, H.Y. Liu, Z.Q. Guo, M.Y. Yang, J.R. Song, H.X. Ma, Two Cu(II)-triadimenol complexes as potential fungicides: synergistic actions and DFT calculations, RSC Adv. 8 (2018) 2933–2940.
[44] P.S. Zhao, X.M. Gao, J. Song, X.J. Sun, W.L. Zeng, Synthesis, characterization, crystal structure and DFT studies on 3-(1H-benzo[*d*][1,2,3]triazol-1-yl)-1-oxo-1-m-tolylpropan-2-yl-nicotinate, Spectrochim, Acta A Mol.Biomol. Spectrosc 79 (2011) 219–225.
[45] A. Thamarai, R. Vadamalar, M. Raja, S. Muthu, B. Narayana, P. Ramesh, R.Raj Muhamed, S. Sevvanthi, S. Aayisha, Molecular structure interpretation, spectroscopic (FT-IR, FT-Raman), electronic solvation (UV–Vis, HOMO-LUMO and NLO) properties and biological evaluation of (2E)-3-(biphenyl-4-yl)-1-(4-bromophenyl)prop -2-en-1-one: experimental and computational modeling approach, Spectrochim, Acta A Mol.Biomol. Spectrosc 226 (2020) 117609.
[46] D.A. Long, Infrared and raman characteristic group frequencies. Tables and charts george socrates John Wiley and Sons, Ltd, chichester, third edition, 2001.price £135, J. Raman Spectrosc. 35 (2010).
[47] S. Shukla, A. Srivastava, P. Kumar, P. Tandon, R. Maurya, R.B. Singh, Vibrational spectroscopic, NBO, AIM, and multiwfn study of tectorigenin: a DFT approach, J. Mol. Struct. 1217 (2020) 128443.
[48] L. Joseph, D. Sajan, R. Reshmy, B.S. Arun Sasi, Y. Erdogdu, K.K. Thomas, Vibrational spectra, structural conformations, scaled quantum chemical calculations and NBO analysis of 3-acetyl-7-methoxycoumarin, Spectrochim, Acta A Mol.Biomol. Spectrosc 99 (2012) 234–247.
[49] L.W. Li, T.C. Cai, Z.Q. Wang, Z.X. Zhou, Y.D. Geng, T.M. Sun, Study on molecular structure, spectroscopic investigation (IR, Raman and NMR), vibrational assignments and HOMO–LUMO analysis of L -sodium folinate using DFT: a combined experimental and quantum chemical approach, Spectrochim, Acta A Mol.Biomol. Spectrosc 120 (2014) 106–118.
[50] M.N. Akhtar, M.A. AlDamen, W. Zierkiewicz, M. Michalczyk, M. Khalid, M. Idrisi, M. Shahid, Synthesis, crystal structure, DFT calculations, molecular docking study and Hirshfeld surface analysis of alkoxido-bridged dinuclear iron(III) complex, Res. Chem. Intermed. 46 (2020) 4155–4171.
[51] D.B. Janakiramudu, D.S. Rao, C. Srikanth, S. Madhusudhana, P.S. Murthy, M. Nagalakshmidevamma, P.V. Chalapathi, C.N. Raju, Sulfonamides and carbamates of 3-fluoro-4- morpholinoaniline (linezolid intermediate): synthesis, antimicrobial activity and molecular docking study, Res. Chem. Intermed. 44 (2018) 469–489.
[52] B. Koohshekan, A. Divsalar, M. Saiedifar, A.A. Saboury, B. Ghalandari, A. Gholamian, A. Seyedarabi, Protective effects of aspirin on the function of bovine liver catalase: a spectroscopy and molecular docking study, J. Mol. Liq. 216 (2016) 8–15.
[53] S. Shahraki, H.S. Delarami, M. Saeidifar, Catalase inhibition by two Schiff base derivatives. Kinetics, thermodynamic and molecular docking studies, J. Mol. Liq. 287 (2019) 111003.
[54] M.S. Ali, J. Muthukumaran, H.A. Al-Lohedan, Molecular interactions of ceftazidime with bovine serum albumin: spectroscopic, molecular docking, and DFT analyses, J. Mol. Liq. 313 (2020) 113490.
[55] F.L. Wu, Q.Q. Lv, Z.H. Wang, D.D. Li, P. Peng, Y. Yin, S.H. Cui, F.H. Wu, 3D-QSAR, molecular docking and molecular dynamics studies of 2,4- diarylaminopyrimidine analogues (DAAP analogues) as potent ALK inhibitors, Lett. Drug Des. Discovery. 14 (2017) 270–286.
[56] R. Adhithya, M. Kullappan, R. Sudha, A. Anand, FtsA as a cidal target for Staphylococcus aureus: molecular docking and dynamics studies, J. Cell. Biochem. 120 (2019) 7751–7758.